Article

Applied Physics

Analysis of temperature-dependent characteristics of a 4H-SiC metal-semiconductor-metal ultraviolet photodetector

CHEN Bin[1,2*], YANG YinTang[1], XIE XuanRong[3], WANG Ning[1], MA ZhenYang[1], SONG Kun[1] & ZHANG XianJun[1]

[1] *Key Laboratory of Ministry of Education for Wide Band-Gap Semiconductor Materials and Devices, School of Microelectronics, Xidian University, Xi'an 710071, China;*
[2] *Xi'an Electronic Engineering Research Institute, Xi'an 710100, China;*
[3] *No. 771 Institute of Microelectronics Technology, Xi'an 710054, China*

We investigate the temperature dependence of current-voltage and spectral response characteristics of a 4H-SiC metal-semiconductor-metal (MSM) ultraviolet photodetector in the temperature range from room temperature to 800 K with two-dimensional (2D) numerical simulator ISE-DESSIS. It is found that the dark current and photocurrent increase with the increasing temperature. For the range of 500–800 K, the dark current increases by nearly a factor 3.5 every 150 K larger than that of photocurrent, leading to a negative effect on photodetector current ratio (PDCR). Nevertheless, the PDCR is still greater than 200 even at 800 K, which exhibits the excellent thermal stability. In addition, the responsivity has an unsymmetrical trend. As temperature rises, it is clear that a remarkable red-shift of 12 nm occurs and overall responsivity is enhanced for longer wavelength. While the short-wavelength response remains relatively independent of temperature. The mechanism of indirect and direct band absorption transition is responsible for temperature-dependent spectrum distribution. These findings provide a significant insight on the design of the MSM detector operated at elevated temperature.

silicon carbide, ultraviolet photodetector, temperature dependence

In despite of having an indirect bandgap, silicon carbide (SiC) has emerged as an appropriate material for the fabrication of ultraviolet (UV)/visible optoelectronic devices over the last few years due to the available substrates [1], the lower defect density and a more mature process technology [2]. Typically, 4H-SiC based UV photodetectors achieve photosensitivity spectrum of 220–380 nm and peak responsivity at around 290 nm. Photodetectors based on Schottky contacts have an enhanced sensitivity to shorter wavelength radiation as well as a reduced response time as no minority carriers are involved [3]. Especially, the metal-semiconductor-metal (MSM) photodetectors possess potential merits of large device bandwidth, small intrinsic capac-

itance, and sub-nanosecond response time. Whilst the planar process of MSM detectors may be accomplished with as little as one photolithography step and allows their monolithic integration with other optical and electronic circuits [4]. Recent achievements include nano-structured MSM photodetector with high peak voltage [5], MSM solar-blind photodetector with fast rise and decay times of 10 ns and 150 ns [6], high responsivity MSM photodetector with 26000 A/W at 8 V bias via a carrier-trapping process [7]. More recently, MSM UV detectors exhibit UV-photo generated current to dark current ratio up to 1.34×10^8 with colloidal nanoparticles [8], realize a photocurrent gain around 40 at 2 V bias using CaF_2 as the insulator [9], and achieve a very low dark current density of 3.84 nA/cm^2 at 5 V bias based on sol-gel-derived TiO_2 films [10]. Most reported

*Corresponding author (email: xidianchenbin@163.com)

devices meet the requirement of optical detection in terms of low dark current, high responsivity and fast response. Up to now, several groups have reported the temperature dependence for photodetectors, including Ge-on-Si p-i-n detector [11], nonreach-through 4H-SiC separate absorption avalanche detectors [12], terahertz quantum-well detectors [13] and Schottky detectors [14]. Lately, the dependence of dark current and response characteristics for GaN-based avalanche photodiodes can be found in [15]. However, a thorough description of temperature dependence of the dark/illuminated current and spectral response of 4H-SiC MSM detectors, particularly quantitative modeling analysis, is still lacking, whereas it can determine the temperature stability and identify the best operating regions. One of the considerable puzzles is the deficiency of temperature-dependent absorption coefficients.

In this work, we use a self-consistent calculation method to establish a numerical model of a 4H-SiC MSM photodetector. With temperature-dependent physical model, an investigation of dark current variation at elevated temperature is carried out via a two-dimensional (2D) device simulator ISE-DESSIS. For the optical features at wide range of temperature, we address an exploratory method to extrapolate the UV absorption coefficients at different temperatures with consideration of the effects of variant phonon population, bandgap narrowing and direct band transition [16]. Finally, the calculated results are verified with relevant experiment and the electrical and optical characteristics of the MSM detector above room temperature (RT) are discussed in detail to evaluate thermal stability for practical application.

1   Methodology

1.1   Device structure and characterization

The cross section of a 4H-SiC MSM photodetector is illustrated in Figure 1. The layer structure consists, from bottom to top, of three parts: an ideal 400-μm n^+ 4H-SiC substrate with doping concentration of 10^{20} cm^{-3}, an n^- epilayer with a thickness of 5 μm and a doping level lower than 10^{16} cm^{-3}, and Au Schottky contacts formed planar interdigital fingers with a height of 80 nm. The fingers of the contact electrodes are 3 μm wide and 500 μm long with a spacing of 3 μm. The optical sensitive area of the UV photodetector is 200 μm× 500 μm.

1.2   Numerical modeling

The analysis of the device behavior at only room temperature does not give detail information about the nature of device reliability and their conduction process. Different from the previous calculation models at room temperature (RT), we must determine the governing physics for the device operation at elevated temperature with consideration of
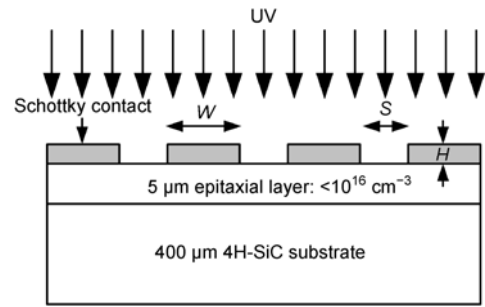

Figure 1   Schematic cross section of a 4H-SiC MSM UV detector.

the temperature effect on dark/illuminated conduct mechanism. In this study, a series of physical models utilized in ISE-DESSIS are the Shockley-Read-Hall (SRH) generation/recombination model including the band-to-band tunneling and the trap-assisted tunneling items, the thermionic emission model, the barrier lowering model and the incomplete ionization model. A more detailed description of the models can be specified in [17] and similar modeling and simulation methods are presented elsewhere [18]. Here, we elaborate on the appropriate models employed for high temperature operation in combination with experiments and published data. Parts of the model parameters used in our calculation are summarized in Table 1.

(i) Dark current simulating model above RT.   An accurate temperature model is indispensable for describing the device performance at elevated temperatures. Hence, hydrodynamic transport model is used to properly model electron transport, energy relaxation and calculate a spatial electron and lattice temperatures. Unlike the drift-diffusion model, a temperature-dependent hydrodynamic Canali model is selected for the high field saturation of the mobility,

Table 1   Temperature-dependent model parameters used in this study [12,16,17]

Parameters	Unit	Value
β_0		1.23
β_{exp}		0.17
$E_{g,0}$	eV	3.359
α	eV/K	3.3×10^{-4}
β	K	0
a	cm	$1.98 \times 10^6 - 4000 \times (T-300)$
b	V/cm	9.46×10^6
c		1.42
$E_{id,0}$ (Γ-M transition)	eV	3.25
θ (Γ-M transition)	K	638
A_{id} (Γ-M transition)		6.2×10^4
$E_{id,0}$ (Γ-L transition)	eV	4
θ (Γ-L transition)	K	3480
A_{id} (Γ-L transition)		1.8×10^6
$E_{id,0}$ (Γ-Γ transition)	eV	5
A_{id} (Γ-Γ transition)		3.2×10^6

which can be coupled with thermal differential equations and boundary conditions:

$$\mu = \frac{\mu_{\text{low}}}{[\sqrt{1+\alpha^2[3k_B/2(T_C-T_L)]^\beta}+\alpha[3k_B/2(T_C-T_L)]^{\beta/2}]^{2/\beta}}, \quad (1)$$

$$\beta = \beta_0 \left(\frac{T}{T_0}\right)^{\beta_{\exp}}, \quad (2)$$

$$\alpha = \frac{1}{2}\left(\frac{\mu_{\text{low}}}{q\tau_{e,c}v_{\text{sat}}^2}\right)^{\beta/2}, \quad (3)$$

where μ_{low} denotes the low field mobility. $3k_BT_C/2$ is the average carrier thermal energy; $3k_BT_L/2$ gives the equilibrium thermal energy. $\tau_{e,c}$ denotes the energy relaxation time, T_C is the carrier temperature, and T_L denotes the lattice temperature. In addition, we model temperature-dependent band gap [17] as

$$E_g(t) = E_{g,0} + \delta E_{g,0} - \frac{\alpha t^2}{t+\beta}, \quad (4)$$

where $E_{g,0}$ is an adjustable parameter, α and β are material parameters. It is important to utilize an appropriate impact ionization model since the MSM detectors are operated with the variation of temperature. The temperature-dependent impact ionization coefficients for electrons are given by [16]

$$\alpha(T,E) = a\exp\left[-\left(\frac{b}{E}\right)^c\right]. \quad (5)$$

It is reported that the coefficient *a* in 4H-SiC varies linearly with temperature and the exponential term is fairly constant [19]. Thermal generation-recombination is important in calculation of electrical characteristics of the MSM photodetector above RT. It is noted that the dominating recombination mechanism in 4H-SiC is a non-radiative capture of carriers by mid-gap defects [20]. We consider the temperature-dependent carriers life times for electron in the course of Shockley-Read-Hall (SRH) recombination, which can be described by [16]

$$\tau_{n,p} = \frac{\tau_0(T/300)^\alpha}{1+N/N_{\text{ref}}}, \quad (6)$$

where $\alpha = 1.7$, $\tau_0 = 5\times10^{-9}$ s, and $N_{\text{ref}} = 6\times10^{15}$ cm^{-3}.

(ii) UV absorption coefficient model above RT. In order to determine the optical features of the detector, we adopt an accurate optical model to compute the net photon flux of the input UV optical signal via multiple vertical photon beams illuminating on the surface of the device. The key input parameters including optical power, wavelength and incidence window are 2.5×10^{-4} W/cm^2, 2.1×10^{-5}–4×10^{-5} cm and 2×10^{-2} cm, respectively. The specification of

the optical generation rate model can be found in our previous work [21]. To the best of our knowledge, the absorption coefficient related to temperature is vital for calculating the characteristics of the photodetector at elevated temperature and general properties of the carrier recombination and transport. Unfortunately, the optical absorption coefficient for 4H-SiC has been mainly studied only at RT. Inspiringly, Galeckas et al. [22] investigated the temperature dependence of 4H-SiC absorption coefficient at 355 nm. A complete wavelength- and temperature-dependent absorption coefficient in UV region is still lacking. Due to an indirect-transition material, for lower absorption coefficients, we calculate the values as a function of doping, temperature and incident photon energy with the Matlab package. The numerical formula is expressed by [23]

$$\alpha_{\text{indirect}} = A_{id}\left[\frac{(\frac{h\upsilon - E_{id}(N,T)-k\theta}{h\upsilon})^2}{1-\exp(-\theta/T)} + \frac{(\frac{h\upsilon - E_{id}(N,T)+k\theta}{h\upsilon})^2}{\exp(\theta/T)-1}\right], \quad (7)$$

where A_{id} is a fitting coefficient with a unit of cm^{-1}, $h\upsilon$ is the incident photon energy, $E_{id}(N,T)$ is energy spacing from the valence band to the conduction band, k is the Boltzmann constant, $k\theta$ denotes the momentum conserving phonon energy. The first term in eq. (7) represents the photon absorption with phonon emission, and the second term represents the photon absorption with phonon absorption. For photon energies higher than band-gap spacing of 4H-SiC, the direct band transition becomes predominant and the absorption coefficient is related to the following expression [24]:

$$\alpha_{\text{direct}} \propto [h\upsilon - E_{id}(N,T)]^2. \quad (8)$$

The energy spacing $E_{id}(N,T)$ and $E_d(N,T)$ are given by [16]

$$E_{id,d}(N,T) = E_{id,d}(N) - 3.3\times10^{-4}\cdot(T-300), \quad (9)$$

$$E_{id,d}(N) = E_{id,d(0)} - 3.4\times10^{-8}\cdot N^{1/3} - 1.17\times10^{-11}\cdot N^{1/2}. \quad (10)$$

2 Results and discussion

2.1 Verification of numerical model

Due to the lack of relevant experimental results of temperature-dependent dark current characteristics of 4H-SiC MSM photodetector, based on the above models, we calculate the dark current characteristics at 293 K and 321 K of a GaAs MSM detector, whose structure is extremely similar to the measured one with the dark current features at different temperatures reported in [25]. The results are illustrated in Figure 2. As is shown, the calculated dark current is consistent with the measured data especially when the reverse voltage is larger than –4 V. To verify the photocurrent model, the calculated and experimental results with 310 nm
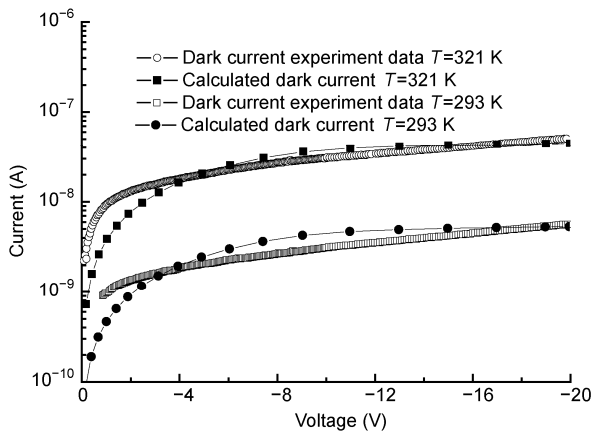
Figure 2 Comparison of calculated dark current of a GaAs MSM detector at different temperature with experimental data [25].

Figure 4 Schematic comparison between the model calculated 4H-SiC absorption coefficient and the measured result [27].

UV illumination are plotted in Figure 3 for comparison [26]. It is found that the calculated photocurrent is somewhat larger than that of measured one with applied bias lower than 5 V. The discrepancy is probably due to the difference between the calculated absorption coefficient based on model and the experimental data. The schematic comparison of absorption model calculated result and measured data is visible in Figure 4, which can account for the phenomenon. However, the approximate agreement between the simulated and experimental results of dark current and photocurrent is achieved, which proves the present numerical models are reasonable.

2.2 The influences of temperature on dark current and photocurrent characteristics of the detector

The dark current characteristics are calculated with temperature ranging from 300 to 800 K. In Figure 5, it is clear that the dark current increases with the bias and temperature. For a voltage lower than 5 V, the every curve achieves a fast increase and then tends to saturation with larger bias. For the variation of temperature, the changes of dark current are
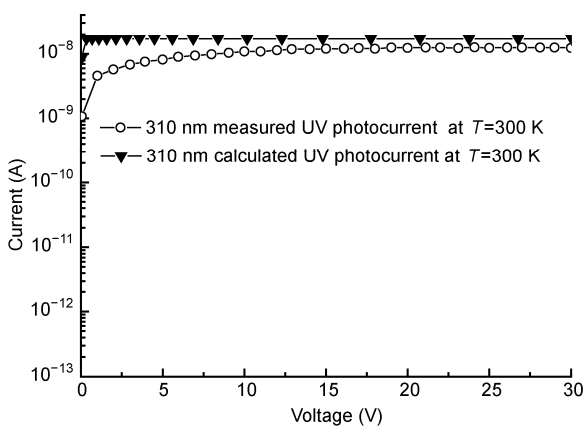

Figure 5 The dark current of 4H-SiC MSM photodetectors versus applied bias with various temperatures between RT and 800 K.

not unified with slightly different dependencies. Specifically, the dark current increases by a factor about 1.7 every 50 K with range of 300–500 K. However, a larger factor about 3.5 is achieved when the detector at 500–800 K. The maximum and minimum dark currents at 800 K and 300 K are 0.646 nA and 2.39 pA. It is clear that the dark current at 800 K is two orders of magnitude higher than that at RT. The band gap narrowing at high temperature and relevant thermionic emission mechanisms are responsible for the phenomenon.

The temperature-dependent photocurrent properties are important characteristics for UV photodetector. As is clearly visible in Figure 6, the variations of photocurrent of MSM UV detector are calculated with the temperature ranging from 300 to 800 K under 330 nm UV illumination. A remarkable increase can be observed at elevated temperatures. With 30 V applied bias, it is found that the photocurrent are 10.8, 12.3, 13.7, 15.2, 16.6, 17.9 and 19.2 nA when the temperature increases from 300 to 800 K. In addition, we can see that the increscent trend of photocurrent is asymmetry. With the range of 300–450 K, the photocurrent rises

Figure 3 Comparison between the calculated photocurrent of the 4H-SiC MSM detector under 310 nm illumination with experiment [26].
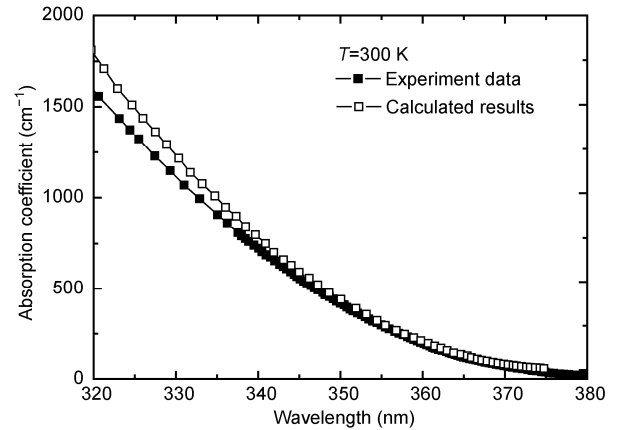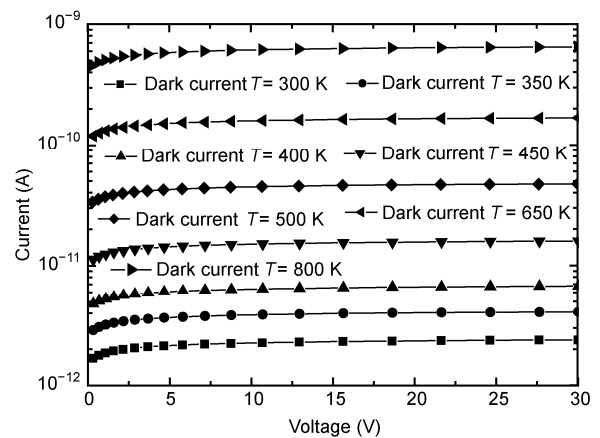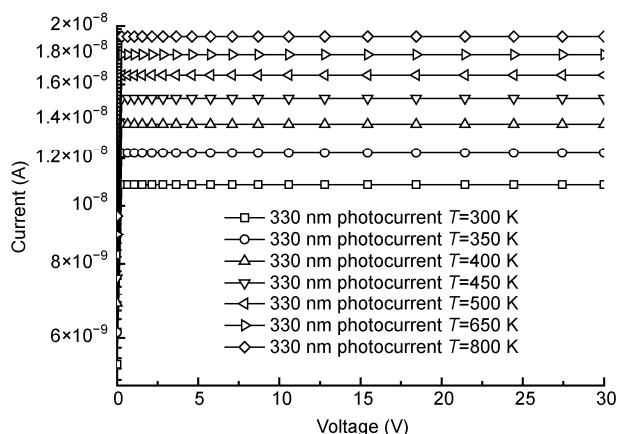
Figure 6   The calculated photocurrent-voltage curves of 4H-SiC MSM detector under 330 nm illumination from RT to 800 K.

Figure 7   PDCR of 4H-SiC MSM detector obtained at various temperatures under a bias of 30 V and 300 nm UV illumination.

very fast and their increment is almost equidistant. Above 450 K, it is obvious that the increase rate of photocurrent slows down. However, the photocurrent at 800 K increases near twice than that of at RT. As the temperature rises, the UV absorption coefficient increases as well. On the other hand, the changes of temperature also have influence on SRH recombination. For the absorption of longer wavelength, the former factor is prevailing as compared with the latter. Therefore, the enhanced absorption effect for the photodetector indicates that more photo-generated carriers can be produced and swept rapidly between electrode contacts to form photocurrent.

Moreover, device performance at elevated temperature can be further estimated by calculation of photodetector current ratio (PDCR), which is defined as [28]

$$\text{PDCR} = (I_p - I_d)/I_d, \tag{11}$$

where I_p denotes photocurrent and I_d dark current. Figure 7 shows the results of PDCR as a function of temperature. The photocurrent is obtained under 300 nm illumination and 30 V applied voltage. It can be seen that the PDCR decreases with the increase of temperature. The PDCR values are larger than 8400 at 300 K and above 5300 at 350 K. Clearly, a steep decrease in PDCR can be observed with further increase in temperature to 450 K. While the temperature is larger than 500 K, the PDCR values tend to saturation. We can see from the Figure 7 that the values decrease gradually from 578 to 249 with temperature up to 800 K. The temperature-dependent current-voltage (*I-V*) characteristics of the detector may account for the decay of PDCR. In contrast to photocurrent, temperature has a relatively direct impact on dark current and the considerable increment in dark current at higher temperature is responsible for the even worse PDCR. However, a comparable value of two orders of magnitude is achieved even at 800 K, which distinctly indicates that the 4H-SiC MSM UV detectors have excellent thermal stability and can be applied under high temperature and harsh condition.
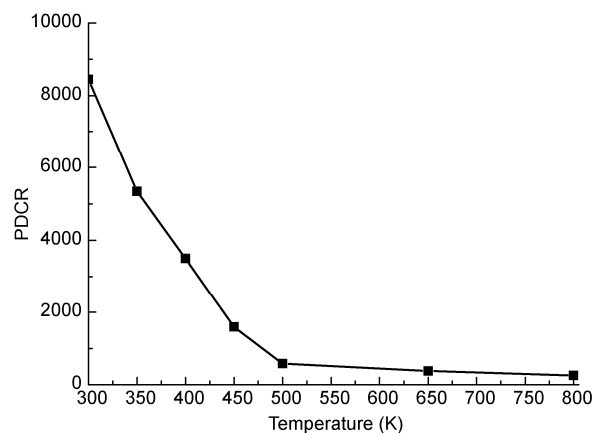
2.3   The influences of temperature on spectral response and quantum efficiency of the detector

Figure 8 shows the responsivity curves of 4H-SiC MSM UV detector at different temperature under 10 V applied voltage. At 300 K, it is found that the responsivity rises with the increasing wavelength. When wavelength is around 290 nm, the responsivity achieves the maximum of 85.2 mA/W. Then, the spectral response decreases gradually and reaches the minimum of 0.048 mA/W at 400 nm. The cutoff of short wavelength (near 240 nm) and long wavelength (near 380 nm) are caused by strong recombination of photon-generated carriers and the decay of optical absorption, respectively. A point to note is that no abrupt spectrum cutoff can be observed with the wavelength ranging from 380 to 400 nm. The reason mainly relates to the fact that the 4H-SiC is an indirect material and does not possess a sharp cutoff edge near the band edge. As is shown in Figure 8, it is found that the peak responsivity increases from 85.2 to 120.3 mA/W, when the temperature increases from 300 to 800 K. A similar behavior of responsivity versus temperature can be found in [29]. Also, it is concluded that the spectral response curves
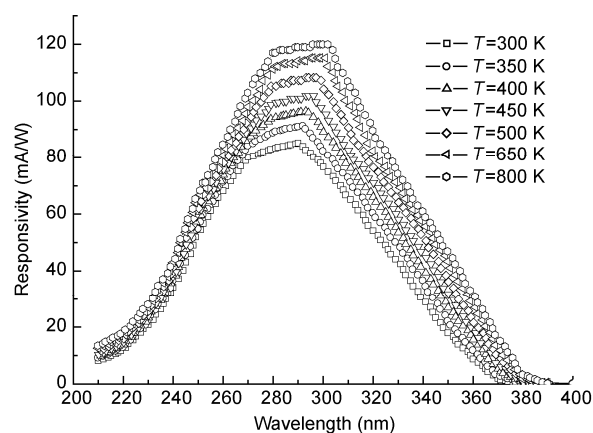

Figure 8   Spectral response of the 4H-SiC MSM photodetector for temperature ranging from RT to 800 K under a bias of 10 V.

become more extensive at the elevated temperature but with discrepant variations. Specifically, a distinct boundary around 270 nm exhibits a nonuniform tendency. When the wavelengths are lower than 270 nm, all curves arranges compactly with the increasing temperature and slight increment of responsivity can be observed, indicating that at short wavelength the spectral response seems to be independent of the temperature. While the wavelength is larger than 270 nm, the variation of responsivity with elevated temperature is more remarkable than the former. Not only does the overall responsivity is enhanced but also the peak increment of responsivity at 800 K is over 41% as compared with RT spectral response. The peak responsivities of the top two curves at 650 K and 800 K are near 299 and 302 nm. Consequently, it is clear that a visible red-shift about 12 nm occurs to longer wavelengths as the temperature increases. The fact that the responsivity shifts to longer wavelength at higher temperature is ascribed to temperature-dependent changes of band gap and optical absorption. Due to thermal expansion, the periodic lattice vibration becomes more violent, which has a profound impact on band structure. When the temperature increases, the band gap narrowing effect is more salient, resulting in the spectrum curves shift towards longer wavelength. Additionally, the elevated temperature varies the phonon distribution and increases the phonon flux. On the other hand, the absorption coefficient is a function of temperature and photon energy. For the wavelength near the band gap, the lower photon energy can be represented by Γ-M indirect band transition in 4H-SiC. The higher the temperature is, the greater absorption will be and, in turn, enhanced responsivity feature is achieved. However, for the high photon energies obtained at short wavelength, the direct band transition is predominant. While the temperature increases, an explosive increment of absorption coefficient effectively reduces the penetration depth of photon owing to the fact that the former is reversely proportional to the latter. Thus, photon-generated carriers cannot form a photocurrent due to intense recombination occurring at device surface. Therefore, the high recombination rate offsets the advantage of higher absorption so that the response curves at low wavelength region remain independent of temperature. Under a bias of 10 V, the quantum efficiencies versus diverse temperatures are sketched in Figure 9. It is noted that all curves, no matter short or long wavelength region, shift upwards as temperature rises. The peak zones of quantum efficiency of the curves locate at 280 nm. The maximum quantum efficiency of 51.82% and the minimum of 36.94% are obtained with corresponding temperature of 800 K and RT, respectively. In comparison with the both, we can find that the peak value of quantum efficiency increases approximately about 41%, indicating that temperature intensely affects the photoelectric conversion process of the detector.
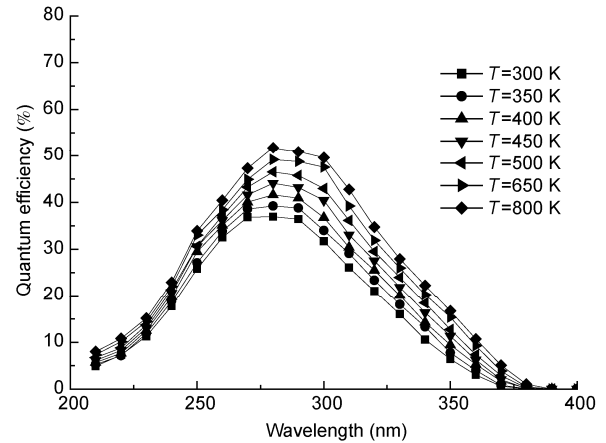

Figure 9 Quantum efficiency of the 4H-SiC MSM detector as a function of wavelength and temperature at 10 V bias.

3 Conclusions

With consideration of temperature-dependent physical model, we investigate the temperature dependence of a 4H-SiC MSM photodetector in terms of dark/illuminated *I-V* features and spectral characteristics in the range of 300–800 K by utilizing a 2D device simulator ISE-DESSIS. The calculations are in good agreement with the measured characteristics, thereby, validating the correctness of our numerical modeling. Up to 30 V bias, a distinct increase of the dark current and photocurrent can be observed as the temperature rises from RT to 800 K. The impact of temperature on dark current becomes predominant as compared with the counterpart, leading to the decrease of PDCR. However, the PDCR value obtained even at 800 K is still greater than 200, which reveals the excellent thermal stability of the detector. Furthermore, it is found that the red shift of responsivity shifts to longer wavelength. For spectral response and quantum efficiency, a noticeable increment with elevated temperature can be found. At 800 K, the maximum responsivity of 120.3 mA/W and peak quantum efficiency of 51.82% can be obtained at 302 and 280 nm, respectively. In brief, the systematic investigations, providing valuable information about temperature-dependent properties of the 4H-SiC MSM UV detector, are of paramount essentiality in the assessment of the device stability and reliability under harsh and high-temperature UV detection condition.

1   Powell A R, Rowland L B. SiC materials-progress, status, and potential roadblocks. Proc IEEE, 2002, 90: 942–955
2   Razeghi M. Short-wavelength solar-blind detectors-status, prospects, and markets. Proc IEEE, 2002, 90: 1006–1014
3   Wright N G, Horsfall A B. SiC sensors: A review. J Phys D, 2007, 40: 6345–6354
4   Ito M, Wada O, Nakai K, et al. Monolithic integration of a metal-semiconductor-metal photodiode and a GaAs preamplifier. IEEE

Electron Device Lett, 1984, 5: 531–532

5 Borsa T, Williams D F, Hale P D, et al. Novel nano-structured metal-semiconductor-metal photodetector with high peak voltage. Jpn J Appl Phys, 2009, 48: 06FD031

6 Wang L K, Ju Z G, Shan C X, et al. MgZnO metal-semiconductor-metal structured solar-blind photodetector with fast response. Solid State Commun, 2009, 149: 2021–2023

7 Liu J S, Shan C X, Li B H, et al. High responsivity ultraviolet photodetector realized via a carrier-trapping process. Appl Phys Lett, 2010, 97: 251102

8 Qin L Q, Shing C, Sawyer S. Metal-semiconductor-metal ultraviolet photodetectors based on zinc-oxide colloidal nanoparticles. IEEE Electron Device Lett, 2011, 32: 51–53

9 Sang L W, Liao M Y, Koide Y, et al. High-performance metal-semiconductor-metal InGaN photodetectors using CaF₂ as the insulator. Appl Phys Lett, 2011, 98: 103502

10 Xie Y N, Huang H L, Yang W F, et al. Low dark current metal-semiconductor-metal ultraviolet photodetectors based on sol-gel-derived TiO₂ films. J Appl Phys, 2011, 109: 023114

11 Balbi M, Sorianello V, Colace L, et al. Analysis of temperature dependence of Ge-on-Si p-i-n photodetectors. Physica E, 2009, 41: 1086–1089

12 Cha H Y, Soloviev S, Zelakiewicz S, et al. Temperature dependent characteristics of nonreach-through 4H-SiC separate absorption and multiplication APDs for UV detection. IEEE Sensors J, 2008, 8: 233–237

13 Tan Z Y, Guo X G, Cao J C, et al. Temperature dependence of current-voltage characteristics of terahertz quantum-well photodetectors. Semicond Sci Technol, 2009, 24: 115014

14 Blank T V, Goldberg Yu A, Kalinina E V, et al. Temperature dependence of the photoelectric conversion quantum efficiency of 4H-SiC Schottky UV photodetectors. Semicond Sci Technol, 2005, 20: 710–715

15 Wang X D, Hu W D, Chen X S, et al. Dependence of dark current and photoresponse characteristics on polarization charge density for GaN-based avalanche photodiodes. J Phys D, 2011, 44: 405102

16 Cha H Y, Sandvik P M. Electrical and optical modeling of 4H-SiC avalanche photodiodes. Jpn J Appl Phys, 2008, 47: 5423–5425

17 DESSIS. 2D Semiconductor Device Simulator. Version 10.0 2005, Integrated Systems Engineering, Zurich

18 Chen B, Yang Y T, Chai C C, et al. Optical coupling optimization in a novel metal-semiconductor-metal ultraviolet photodetector based on semicircular Schottky electrodes. J Semicond, 2012, 33: 054010

19 Raghunathan R, Baliga B J. Temperature dependence of hole impact ionization coefficients in 4H and 6H-SiC. Solid State Electron, 1999, 43: 199–211

20 Bergman J P, Kordina O, Janzen E. Time resolved spectroscopy of defects in SiC. Phys Status Solidi A, 1997, 162: 65–77

21 Chen B, Yang Y T, Chai C C, et al. Two-dimensional numerical computation of the structure-dependent spectral response in a 4H-SiC metal-semiconductor-metal ultraviolet photodetector with consideration of reflection and absorption on contact electrodes. J Semicond, 2011, 32: 084001

22 Galeckas A, Grivickas P, Grivickas V, et al. Temperature dependence of the absorption coefficient in 4H- and 6H-silicon carbide at 355 nm laser pumping wavelength. Phys Status Solidi A, 2002, 191: 613–620

23 Nallet F, Planson D, Isoird K, et al. Comparison of static, switching and thermal behavior between a 1500 V silicon and silicon carbide bipolar diodes. Proc Int Semicond Conf, 1999, 1: 195–198

24 Lindefelt U. Doping-induced band edge displacements and band gap narrowing in 3C-, 4H-, 6H-SiC, and Si. J Appl Phys, 1998, 84: 2628

25 Averine S, Chan Y C, Lam Y L. Evaluation of Schottky contact parameters in metal-semiconductor-metal photodiode structures. Appl Phys Lett, 2000, 77: 274–276

26 Yang W F, Zhang F, Liu Z G, et al. Effects of annealing on the performance of 4H-SiC metal-semiconductor-metal ultraviolet photodetectors. Mater Sci Semicond Proc, 2008, 11: 59–62

27 Sridhara S G, Devaty R P, Choyke W J. Absorption coefficient of 4H silicon carbide from 3900 to 3250 angstrom. J Appl Phys, 1998, 84: 2963

28 Chang W R, Fang Y K, Ting S F, et al. The hetero-epitaxial SiCN/Si MSM photodetector for high-temperature deep-UV detecting applications. IEEE Electron Device Lett, 2003, 24: 565–567

29 Sou I K, Ma Z H, Zhang Z Q, et al. Temperature dependence of the responsivity of ZnS-based UV detectors. J Cryst Growth, 2000, 214: 1125–1129